Mapping the Distribution of Ion Positions as a Function of Quadrupole Ion Trap Mass Spectrometer Operating Parameters to Optimize Infrared Multiphoton Dissociation

Philip M. Remes and Gary L. Glish*

Department of Chemistry, University of North Carolina at Chapel Hill, Chapel Hill, North Carolina 27599-3290

Received: October 9, 2008; Revised Manuscript Received: February 21, 2009

Infrared multiphoton dissociation (IRMPD) combined with ion trajectory simulations has been used to obtain probability maps of ion position as a function of different operating parameters in a quadrupole ion trap mass spectrometer. The factors that contribute to the depth of the pseudopotential trapping well are analyzed, and their effects on the efficiency of IRMPD are demonstrated. Ion trajectory simulations are used to substantiate experimental results and demonstrate in greater detail the dynamic nature of the ion population's positional distribution. In particular, it is shown that the so-called "q_z value" used during photodissociation can be of great consequence, as can the frequency of ac trapping voltage applied to the ring electrode. The results reveal that parameters which increase the pseudopotential well have the effect of decreasing the size of the ion cloud and maximizing overlap between the irradiating laser and the ions. Thus, while the common understanding of IRMPD dictates otherwise, IRMPD fragmentation efficiencies really depend on many ion trap operating parameters, much as collision-induced dissociation does.

Introduction

Lasers have been used as a tool for the photodissociation of ions in mass spectrometers for at least 35 years.[1] Trapping instruments such as quadrupole ion trap mass spectrometers (QITMS) in particular are advantageous for photodissociation because they serve to hold the ions in the laser path, allowing multiphoton processes such as infrared multiphoton dissociation (IRMPD). Lasers and trapping instruments have been employed in a variety of applications, ranging from determination of radiative and collisional cooling rates,[2−4] ion tomography,[5−7] primary structure elucidation of proteins and peptides,[8−13] assistance in electron capture dissociation (ECD),[14] and finally more recently in IR action spectroscopy.[15−19] Of fundamental importance in any laser photodissociation experiment is that the volume defined by the ion trajectories, henceforth denoted as the ion cloud, intersects the irradiating volume of the laser. Satisfying the condition of ion/laser overlap might seem trivial, necessitating only optimization of the laser alignment optics, until the dynamic nature of the ion cloud in a QITMS is considered. As will be discussed in detail in later sections, in a QITMS the force pushing an ion toward the center of the trap (where the laser is typically aimed) depends on a number of instrumental parameters. Any alteration of this force is reflected in the dimensions of the ion cloud. Thus, when the laser beam profile is near the same size as the ion cloud radius, a change in instrumental parameters can have an effect on the efficiency of photodissociation. This effect is more pronounced when the laser beam is focused to very small diameters relative to the ion cloud size but is also noticeable with larger diameter laser beams, due to the Gaussian (nonhomogenous) beam intensity profile. Ion cloud dimensions were measured previously in a QITMS for an ion tomography experiment.[7] The ion radial and axial distributions were mapped by scanning the position of a XeCl excimer laser and measuring fragmentation efficiency. The purpose of that study was to correlate ion cloud dimensions to space charge related mass shifts; therefore the parameter that was varied was the number of ions trapped, and the other trapping parameters were kept constant. The present work will demonstrate that various other QITMS instrumental parameters affect the efficiency of IRMPD, contrary to conventional wisdom.[13,20−22] A combination of experimental and theoretical methods is used to map the distribution of ion positions as a function of these parameters.

* To whom correspondence should be addressed. Phone: 919-962-2303. E-mail: glish@unc.edu.

Theory

Quadrupole Ion Trap Parameters. A brief overview of quadrupole ion trap theory will be introduced to present the concept of the q_z parameter for later discussion. Several publications describe in detail how the equation of an ion's motion in a quadrupolar field may be derived, starting from the basic relations

$$\vec{F} = m\vec{a} = -e\vec{\nabla}\Phi \tag{1}$$

where F is force, m is mass, a is acceleration, e is the charge constant, and $\nabla\Phi$ is the derivative of the potential with respect to all space.[23−25] The result of these derivations describing an ion's motion may be written in the general form of the Mathieu equation, given in eq 2

$$\frac{d^2z}{d\xi^2} + (a_z - 2q_z \cos 2\xi)z = 0 \tag{2}$$

The positional coordinate in the axial direction of the QITMS has been given by z, since ejection processes occur in this direction. A similar equation can be written for radial position or r. The dimensionless parameters ξ, a_z, and q_z are given in the following equations

10.1021/jp808955w CCC: $40.75
Published on Web 03/25/2009

$$\xi = \Omega t/2 \tag{3}$$

$$a_z = -\frac{16eU}{m(r_0^2 + 2z_0^2)\Omega^2} \tag{4}$$

$$q_z = \frac{8eV}{m(r_0^2 + 2z_0^2)\Omega^2} \tag{5}$$

where Ω is the radio frequency (rf) trapping voltage frequency (in radians per second), t is time, U and V are the amplitudes of the dc and maximum zero to peak rf voltage applied to the ring electrode of the trap, e is the fundamental unit of charge, m is mass, and r_0 and z_0 are the radial and axial dimensions of the trap. Solutions to Mathieu's equation that result in stable ion trajectories in the QITMS may be mapped out in a_z and q_z space. From such an analysis comes the familiar observation that if U equals 0, as is common practice, then an ion has a stable trajectory in the QITMS at values of $q_z < 0.908$. The method of mass-selective instability[26] makes use of the stability boundary at $q_z = 0.908$ and increases the rf voltage to sequentially eject ions from the trap in order of mass-to-charge ratio.

The q_z parameter is of great practical value in QITMS experiments as it allows the calculation of the voltage required to eject an ion from the trap; it also allows the calculation of an ion's fundamental frequency of oscillation, known as its secular frequency. A supplementary voltage applied to the end-cap electrodes at this frequency can be used to resonantly excite the ion. Resonance excitation increases the kinetic energy of the ion, which can be used at low voltages to activate the ion through collisions with the He bath gas, or can be used at higher voltages to eject the ion from the trap.[27]

Pseudopotential Well Model. The pseudopotential well model describes some of the factors controlling the size of the ion cloud. Briefly, this model assumes that ion motion in a QITMS can be decoupled into a low-frequency oscillation at the ion's secular frequency, ω, and a high frequency ripple at $\Omega \pm \omega$, where Ω is the drive frequency.[28] At low rf values ($q_z < 0.4$) the high-frequency ripple can practically be ignored.[23,29,30] Under these conditions an ion's motion can be approximated as that of a harmonic oscillator in a parabolic potential well, where the depth of the well in the axial direction is D_z, as in eq 6

$$D_z = \frac{mq_z^2\Omega^2 z_0^2}{16e} \tag{6}$$

Equation 6 can be used for the radial direction as well, substituting q_r and r_0 for q_z and z_0. If the axial and radial dimensions of the trap were equal, then D_z would be $4D_r$, the depth of the well in the radial direction, because $q_z = -2q_r$. The q_r term is the Mathieu stability parameter for the radial direction, analogous to q_z in the axial direction. The $q_z = -2q_r$ relation arises from weighting coefficients from solving Laplace's equation for a three-dimensional quadrupolar geometry. However, the axial and radial dimensions of a trap are not equal; the theoretical relation between axial and radial dimensions for a QITMS is $r_0^2 = 2z_0^2$. Under this condition $D_z = 2D_r$. The electrodes used in this work were from an ITMS and have an 11% axially stretched geometry, where $r_0 = 1.00$ cm and $z_0 = 0.783$ cm, and so the actual relationship between axial and radial well depths is $D_z = 2.45D_r$.

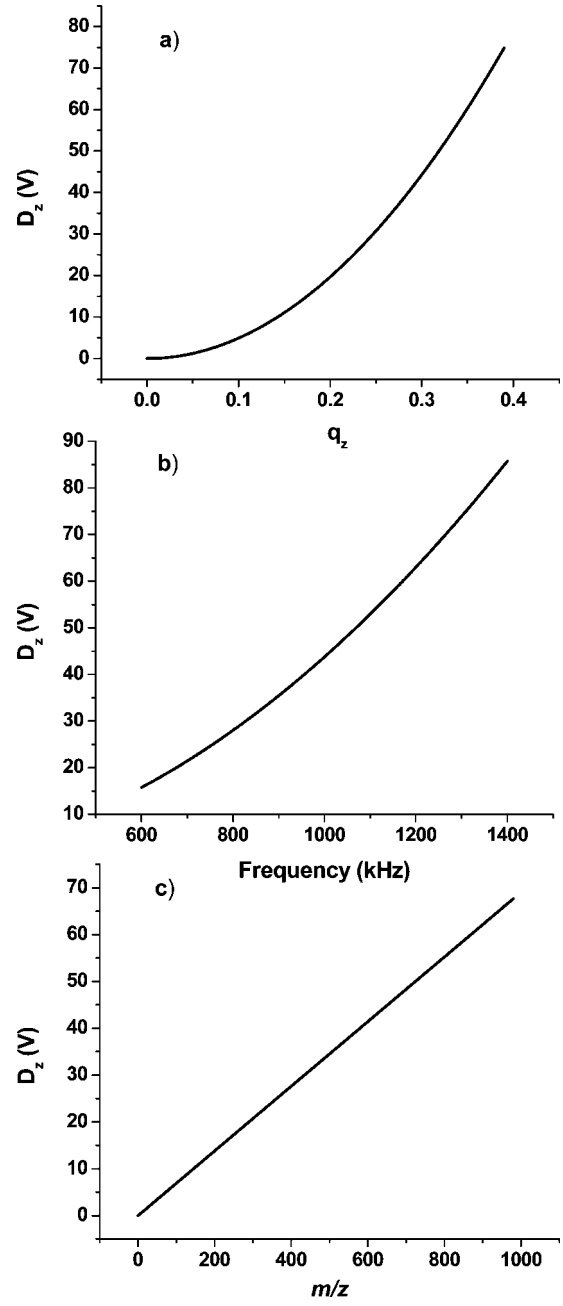

Figure 1. Pseudopotential trapping well depth as a function of (a) q_z value, for 445 Da, $\Omega = 838$ kHz, (b) rf trapping frequency, for 445 Da, $q_z = 0.25$, and (c) ion mass-to-charge, $q_z = 0.25$, $\Omega = 838$ kHz.

In Figure 1, the axial pseudopotential well depth has been plotted as a function of various ion trapping parameters using eq 6. In Figure 1a the q_z value is varied for a 445 Da ion at a trapping frequency of 838 kHz; Figure 1b has the rf trapping frequency varied for a 445 Da ion at $q_z = 0.25$, and in Figure 1c ion mass-to-charge is varied at $q_z = 0.25$ and rf trapping frequency of 838 kHz. The restoring force pushing an ion toward the center of the ion trap (the "bottom" of the pseudopotential well) increases with potential as in eq 1; therefore, all other parameters being equal, a smaller ion cloud is expected for traps operating at higher rf voltage (q_z), at higher frequency, and for ions of larger mass-to-charge ratios. The depth of the pseudopotential well approaches zero at values of the parameters that might be considered close to typical, especially for IRMPD. If

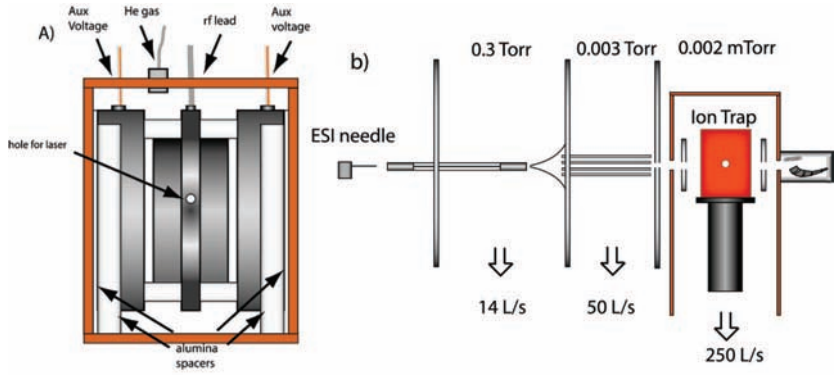

Figure 2. (a) Cut-away, side view of ion trap electrodes secured inside a copper holder. (b) Diagram of entire instrument, with trap holder mounted on top of closed-cycle helium refrigerator.

a small well depth leads to a diffuse ion cloud, then trapping conditions may need to be adjusted for optimum dissociation efficiency.

The experiments in this study will vary q_z value, rf drive frequency, and ion mass-to-charge ratio to examine the effects of these parameters on the positional distribution of ions in the trap. Similar to previous studies,[7,31] laser dissociation will be used as a tool to observe these changes. In the present study, however, IRMPD with a CO_2 laser is used, and the operating parameters of the QITMS are varied. There is no provision for scanning the position of the laser beam; the beam is kept centered in the middle of the trapping volume, and changes in the efficiency of dissociation are monitored as q_z value is varied. The changes in dissociation efficiency are linked to changes in ion cloud size because as an ion's radius of oscillation gets smaller it will spend more time inside the laser beam absorbing photons and will more readily dissociate. When an ion is stored in the QITMS at conventional He bath gas pressures (~1 mTorr), collisional processes effectively bring the ion's vibrational temperature into equilibrium with the room temperature He bath gas.[4,32,33] During IRMPD, when an ion is not being activated inside the laser beam it is being deactivated with a collisional cooling rate constant on the order of 400 s^{-1}. This rate constant is derived from a plot of internal energy (or related quantity) versus time fitting to an exponential decay.[4,34] Therefore, with a smaller ion cloud the IRMPD process will compete better with the collisional cooling effect of the bath gas, resulting in more dissociation.

Experimental Methods

Instrumentation. The instrument that was used in these experiments was a custom-built design made for cold-temperature IR spectroscopy experiments. The quadrupole ion trap was a Finnigan ITD set of electrodes with a 3.175 mm hole drilled in the ring electrode for the laser to enter the ion trapping volume. The ion trap was mounted on top of a Sumitomo RDK-408S 10 K closed-cycle helium cold head. The ion trap was held in place by a copper enclosure bolted to the second stage of the cold head. Copper was the material of choice for this enclosure due to its high thermal conductivity. Electrical isolation of the end-cap electrodes from the copper enclosure was obtained by using high alumina ceramic spacers (McMaster-Carr Supply Company, Chicago, Il), which have good thermal conductivity.

Figure 2a is an illustration of the ion trap in its holder, with one side of the holder box taken away for clarity. The temperature of the system can be regulated with a Lakeshore 340 controller, which controls a 100-W heater attached to the cold head and receives feedback from a silicon diode mounted on the ion trap holder. A second copper piece, a cylinder that encompasses the entire trap holder, was bolted to the body of the cold head. This cylinder can cool down to ~75 K and acts as a shield to isolate the trap holder from the blackbody radiation of the room-temperature vacuum housing. An instrument diagram, as configured for electrospray ionization (ESI), is shown in Figure 2b. So far the system has reached a lowest temperature of 23 K. Because the present experiments were performed at room temperature, no cooling was necessary and the tops of the copper enclosures were removed to allow direct measurement of the pressure of He in the trapping volume (i.e., no conductance limited flow between the ion trap electrodes and pressure gauge). The He pressure was 7×10^{-4} Torr. Holes of 6.35 mm are drilled in the cylinder, on-axis with the entrance and exit holes of the ion trap, to allow ions to enter and leave the mass spectrometer. Ion lenses placed halfway between the first and second stage enclosures serve to focus incoming ions into the trap and focus ejected ions into a channeltron-type electron multiplier for detection (Burle Industries, Inc., Lancaster, PA.). Two more 6.35 mm holes, placed 90 degrees from those described above, allow a laser beam to traverse the instrument and interact with the ions inside the ion trap.

The high vacuum portion of the instrument, where the ion trap is located, was pumped by a 250 L/s Varian (Palo Alto, CA.) 301 Navigator turbo pump. The base pressure was 8.0×10^{-8} torr, measured by a cold cathode gauge. Separated from the high vacuum region by a 2.0 mm hole was a multiuse space, pumped by a 50 L/s Varian Turbo-V 81 turbo pump. The plate defining the 2.0 mm hole also serves to gate ions, that is, to apply a focusing voltage when ions are to be injected into the ion trap and to a apply a large blocking voltage at all other times.

When analysis of ions produced by electron ionization (EI) was desired, the octapole was removed and a TSQ 70 EI source was inserted in that space and sealed off from the capillary region. Base pressure in the EI source region is 8.0×10^{-8} Torr. Electron energy was set to 70 eV, and the EI source is floated at 20 V. Sample vapors were leaked into the source at $\sim 2 \times 10^{-6}$ Torr through a side arm fitted with a metering valve.

When nano-ESI was desired, this multiuse space houses an octapole ion guide and was separated from a high pressure/desolvation region by a skimmer with a 0.6 mm orfice. The ions were transferred through the multiuse space with a custom-built octapole ion guide. The octapole was driven by an rf oscillator built by the UNC electronics shop, on the basis of a previously described design.[35] When the skimmer was mounted, the pressure in the multiuse space was 3×10^{-3} Torr, and the

base pressure in the main vacuum chamber was 2×10^{-6} Torr. The high pressure region (0.35 Torr) contained a 20.32 cm glass capillary traversed by a ~400 μm diameter channel. A voltage was applied to a metal cap on the end of the capillary to help focus ions into the skimmer, while another metal cap on the atmospheric side of the capillary provided a place to apply the −1000 V for nano-ESI of a sample in a pulled glass needle.

The signal from the electron multiplier was amplified and filtered, before acquisition by a National Instruments (NI) PXI-6289 M-Series DAQ card (Austin, TX). Supplemental waveforms were applied to the end-cap electrodes of the ion trap with a NI 5412 arbitrary waveform generator. The main rf voltage applied to the ring electrode for ion trapping was produced by a 838.5 kHz, 0.285 $V_{0\text{-}p}$ sine wave from a NI 5404 function generator, which was modulated with a 0−10 V DC signal before being sent to a 100-W power amplifier and finally stepped up to its final level by the rf coil from a Finnigan ITMS system. All aspects of the experiment were controlled by a custom software program written in LabVIEW 7.1.

Sample Solutions. The protonated molecules of tetracycline, the peptide glycine-histidine-lysine (GHK), and the peptide phenylalanine-leucine-leucine-valine-proline-leucine-glycine (FLLVPLG) were produced by nano-ESI. The molecular ion of *n*-butylbenzene was produced by 70 eV EI. The ESI sample concentrations were 100−200 μM in 75/20/5 methanol/water/acetic acid. Tetracycline, GHK, and *n*-butylbenzene were purchased from Sigma Aldrich (St. Louis) and FLLVPLG was custom synthesized by Bayer Corp. All samples were used without any purification.

CO_2 Laser. The CO_2 laser used for IRMPD was a continuous wave 10.6 μm, 0−100 W, Synrad Firestar f100. A pulse-width modulated (PWM) control signal of 1 μs pulses at 5 kHz continuously preionized the CO_2 gas to just below the lasing threshold, increasing laser reliability. Further increases in pulse width cause laser emission. The laser output was triggered by a signal from the runtime software at the appropriate time in the experiment. The laser beam was delivered with 3 silicon mirrors and focused to the center of the ITMS with a 38.1 cm focal length ZeSe lens. Great care was taken to ensure that the laser beam passed through the center of the trapping volume. This could be done more easily than in some instruments because when aligned, the beam traverses the entire instrument and hits a water cooled, anodized aluminum beam dump on the other side. Laser alignment was checked each day and tended to stay constant. The manufacturer specified beam quality was TEM_{00}, with a width of 3.5 mm and a 4 mR full angle divergence. The theoretical beam full width at half-maximum at the center of the trap was therefore (half angle divergence × focal length) equal to 0.76 mm. This was verified experimentally by using a razor blade mounted on a precision translation stage to find the positions where the beam power was attenuated by 7 and 93%, and dividing this distance by $\sqrt{2}$. The average of 3 measurements obtained in this manner was 0.78 ± 0.02 mm.

IRMPD Method. The QITMS was filled with He to a pressure of 7.0×10^{-4} Torr. Ions were gated into the ion trap with a high voltage switching circuit for ~10−50 ms. The gating circuit has no provision for automatic gain control,[23,36] so the gate time was chosen to give a moderately high ion signal but not so high that any space charge effects, indicated by mass shifts, were apparent. Ions of lower mass-to-charge than the parent ion were ejected from the trap by raising the rf level to the appropriate value, and any higher mass-to-charge ions (mostly $[M+Na]^+$) were ejected by applying a supplementary ac voltage to the end-cap electrodes at the appropriate frequency and lowering the rf level. The ions were then allowed to cool for 20 ms to ensure equilibrium kinetic and internal energy levels. The CO_2 laser was then turned on for 30 ms, after which the ions were ejected and detected mass selectively with resonance ejection at a q_z of 0.906, slightly less than the stability boundary at $q_z = 0.908$. Each spectrum was the average of 25 scans. Generally, each curve in the data reported here was the average of 5 separate experiments taken on a single day, and error bars were calculated as 95% confidence intervals. The rf level during irradiation by the laser was varied from one spectrum to the next with a computer-run script. The rf levels used corresponded to q_z values ranging from 0.05 to 0.60. When it was necessary to change the frequency of the main drive rf, the location of the tap on the secondary coil of the rf amplification tank circuit was changed and capacitors were added or removed. The new resonant frequency of the system was characterized, and the frequency of the trapping rf function generator was changed to the new resonant value. A new mass scale calibration was then made at the new frequency using a capacitive pickup to monitor the rf voltage levels.

Ion Trajectory Modeling. The purpose of the ion trajectory modeling was to obtain a more complete understanding of how different instrumental parameters affect ion motion. Modeling was done using SIMION 7.0[37] on a 3057 MHz, Pentium 4 personal computer. The QITMS electrodes were simulated with a 797 × 345 × 1 array that was cylindrically mirrored. Grid scaling was set to 0.05 mm/grid unit. Ion motion was started randomly in time over one rf cycle and randomly in position within a 0.50 mm sphere in the center of the trap.

Initial kinetic energy was set to 0.15 eV ± 20% in a random direction. This value was chosen based on separate simulations characterizing the kinetic cooling of an ion for extended periods of time while subjected to millitorr pressures of helium. 445 Da ions at various kinetic energies up to as great as 25 eV were all observed to relax down to values in the 0.1−0.2 eV range. The ions therefore have slightly higher kinetic energy than thermal, which is 0.039 eV at 300 K. Most of the kinetic relaxation takes place in the first 10 ms, with equilibrium levels being reached by ~15 ms for all conditions except low pressure (1×10^{-4} Torr He). For all simulations, the effect of bath gas collisions on ion velocity was taken into account with a 3d hard sphere collision model that uses a Maxwell−Boltzmann distribution of bath gas velocities and a variable mean free path based on a user specified temperature, pressure, and ion collision cross section.[38] The collision cross section used in these simulations was approximated by the relation $\sigma = 50(M/100)^{2/3}$ where σ is ion collision cross section in square angstroms and M is ion mass in Da.[39]

Ions trajectories were simulated for 1 ms with a time resolution of ~5 ns. 100 ions were independently simulated at rf levels corresponding to q_z values of 0.05−0.90, with a step size of 0.05. The amount of time that an ion spent in various parts of the trap was recorded and averaged for each q_z value and was then used to create probability maps of ion position. The plot in Figure 3 is an illustration of how much time an ion spends in each of 30 concentric volumes. Each transition from red to gray contains 10 cylinders, although they are not all clearly visible at this scale. Each volume in Figure 3 is 0.05 mm thick; thus volume 1 is the solid cylinder from 0 mm to 0.05 mm away from the center, and volume 2 is a hollow cylinder from 0.05 mm to 0.10 mm away from the center, etc. The 30 cylinders are collectively the largest ion trapping volume that a laser beam could possibly irradiate, because the hole in the ring electrode is ~3 mm.

Figure 3. Close up of center of SIMION electrode array used to simulate ion trajectories. The time an ion spends in each of 30 cylinders in the center of the trap was recorded to produce a distribution of probability as a function of radius. An ion trajectory at $q_z = 0.10$ is shown, where the ion color is changed in each of the 30 cylinders for emphasis. The blue trace on the top and bottom of the cylinders is the ion path outside of the cylinders. The left and right electrodes are the end-caps through which ions enter and exit the trap. The top and bottom electrodes are actually one cylindrical ring electrode where the trapping voltage is applied.

To attempt to validate the modeling, several checks were performed. A theoretical model was fit to the experimental data by assuming that IRMPD fragmentation efficiency depends on the probability of the ion being within the laser beam, as is described below. Two other validations of the modeling were comparing collision frequency and the axial cloud size from the literature to SIMION determined values. The number of collisions per experiment for the tetracycline simulation was determined to be 23.1 collisions/ms, during normal "storage" q_z values of 0.05−0.60. This is in good agreement with the value of 20 collisions/ms reported previously,[24] although this number should vary depending on ion cross section. Collision rate has a direct effect on collisional cooling rate constant; higher pressure has been shown yield higher rate constants.[4,34] A previous study determined the ion cloud radius to be 0.60 mm in the axial direction for an ion of 105 Da, at a q_z of 0.30, and a pressure of 1.75×10^{-4} Torr.[7] These conditions were simulated in SIMION, and only the axial position of the ions was recorded. The result showed an ion cloud full-width-half-maximum radius of 0.57 mm, in good agreement with the experiment.

Fragmentation Efficiency. In experimental IRMPD spectra, the definition used for fragmentation efficiency (FE) is given in eq 7

$$\mathrm{FE} = \frac{\sum_i F_i}{\sum_i F_i + P} 100 \qquad (7)$$

where FE is fragmentation efficiency, F_i are the intensities of each of the fragment ions produced from IRMPD, and P is the parent ion intensity after IRMPD, so that FE equals 100% when the parent ion has been completely dissociated. Equation 7 does not take into account the abundance of the original precursor ion, as this was found to be unnecessary. Excitation of by the laser does not cause appreciable kinetic excitation of the parent or product ions, such that MS/MS efficiency (fragment ion abundance divided by original precursor ion abundance) is the same as fragmentation efficiency for these experiments. Using peak heights vs peak areas does not affect the results.

To confirm that the SIMION modeling was providing accurate results, a method of computing simulated fragmentation efficiency was devised. The simulations were then compared with the experimental results. The fragmentation efficiency is expected to be a function of the probability of finding the ion in the laser beam volume multiplied by a constant (C), which is dependent on molar absorptivity and the critical energy of dissociation for the ion. Equation 8 gives this simulated fragmentation efficiency

$$\mathrm{FE} = \frac{\sum_{i=0}^{i=radius} t_i}{T} \cdot C \cdot 100\% \qquad (8)$$

FE is fragmentation efficiency, t_i is the time spent in ion volume i of the 30 volumes that were recorded, T is total time, and C is a constant. The times spent in volumes 0 up to some critical radius (the laser beam radius) are summed: beyond this critical radius the calculation assumed that the rate of collisional cooling is greater than the rate of IR activation, resulting in no dissociation. The SIMION probability maps described in the Ion Trajectory Modeling section were used with eq 8 to generate a theoretical fragmentation efficiency. Generally, for a given ion trap pressure, C was the same, and the critical radius was varied for each laser power used, from 0.10 to 0.50 mm. This is because as laser power increases an ion absorbs more photons per unit time, thus less time is needed for dissociation to occur. Increased laser power, therefore, should cause the ions at larger radii to absorb enough photons to dissociate.

Results and Discussion

Effect of rf Voltage on Ion Cloud Size. The result of holding laser power constant for the protonated tetracycline parent ion and increasing the rf voltage level (q_z value) is shown in Figure 4 for several laser indicated laser powers. Clearly as q_z value is increased, the parent ion is dissociated more efficiently. Presumably this is because at higher q_z values the ions are experiencing a stronger restoring force (see eq 6) pushing them toward the center of the trap, which increases the overlap of the ion cloud with the laser beam. At high laser power, fragmentation efficiency levels off at a maximum value around $q_z = 0.3$. At lower laser powers, fragmentation efficiency keeps increasing past a q_z of 0.3, although at a slower rate. Lower laser power effectively allows more "resolution" in the observation of ion cloud size, since at higher laser powers an ion may absorb enough photons to dissociate even away from the center of the laser beam profile. Rf heating should not be a factor, since it has already been shown in a thermal dissociation experiment in a QITMS that rf level did not significantly affect the level of dissociation.[40]

Fundamentally it might be expected that the nature of the ion/molecule collisions at different rf levels would change;

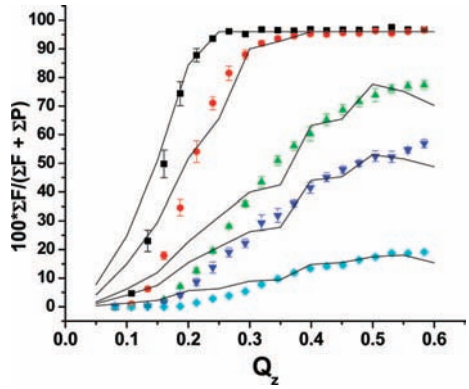

Figure 4. Experimental fragmentation efficiency vs q_z value for tetracycline at various laser powers. The diamond (◆) is 12 W, down-triangle (▼) is 13.5 W, up-triangle (▲) is 15 W, circle (●) is 17.5 W, and square (■) is 20 W. Fits to a calculated fragmentation efficiency are shown in solid, using eq 8.

higher average ion kinetic energies are predicted from the pseudopotential model as q_z increases.[28] The effect this could have on IRMPD is a complex problem; however, a few comments can be made about ion/neutral collisions in general. The most probable outcome of an ion/neutral collision changes as a function of ion internal energy and relative kinetic energy. At low ion internal energy and high relative kinetic energy, heating is expected, while at high ion internal energy and low relative kinetic energy, cooling is more probable.[32,41] Low and high ion internal energy is relative to thermal equilibrium with the bath gas, while low and high relative kinetic energy is relative to the relative kinetic energy of the bath gas collisions. Any increase in ion/neutral collision rate should increase the rate constant for internal energy heating or cooling, whichever is the dominant effect at the current conditions. For the IRMPD experiments in question, while a higher internal energy might be expected as q_z, and thus relative kinetic energy is increased, the thermal dissociation experiments show that this effect is not discernible.

Ion Trajectory Simulations. The theoretical values calculated from SIMION results are also plotted in Figure 4. This fitting of experimental and simulated fragmentation efficiency shows that the changes in fragmentation efficiency with q_z value can indeed be explained by changes in ion cloud size. It would be difficult to try to extract an ion cloud size directly from the experimental data, although it seems fair to conclude qualitatively that the ion cloud is getting smaller as q_z increases. It can be assumed that the ion cloud diameter is on the scale of the laser beam waist of 0.78 mm and is fully contained within this area at higher q_z, but it would be hard to be more precise. A more quantitative ion cloud size can be determined through examination of the calculated results.

The probability of finding a protonated tetracycline ion (445 Da, collision cross section of 1.56×10^{-18} m^2, 7.0×10^{-4} Torr) at a given radius is plotted in Figure 5 as a function of q_z value. There are several features of interest in this plot. At low q_z the ion cloud is spread out over a greater volume and then progressively gets smaller until q_z reachs a value of about 0.4. The ion cloud size stays fairly constant until $q_z = 0.7$ at which point it starts to experience higher amplitude excursions from the center of the trap. It may be significant that ion cloud size stops shrinking once past $q_z = 0.4$ because this is the limit beyond which higher order ion oscillations have appreciable amplitude and the pseudopotential model is not valid. It is also interesting that the peak of ion probability is not at the very center of the trap but rather close to a radius of 0.25 mm. This

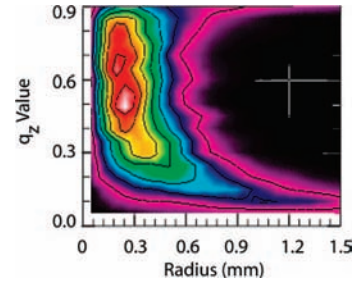

Figure 5. Calculated probability distribution for ion position at various q_z values for protonated tetracycline ion (445 Da, 1.56×10^{-18} m^2, 7.0×10^{-4} Torr). The difference between probability values for each line is 0.02. Therefore, the area at the far right is at a probability of 0.0, while the peak at a radius of 0.3 mm and q_z value of 0.5 is a probability of 0.14−0.16.

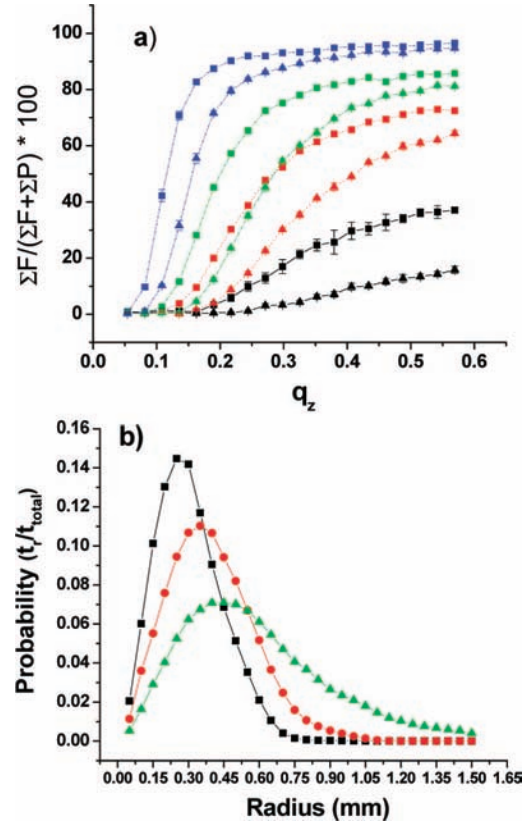

Figure 6. (a) Fragmentation efficiency versus q_z value for n-butylbenzene molecular ion at 7.0×10^{-4} Torr, for several laser powers and trapping frequencies. Squares are 1148 kHz and triangles are 844.5 kHz. Lines of the same type/color are the same laser power. (b) SIMION modeling of ion probability (time at radius r divided by total time) vs distance from center of trap at $q_z = 0.30$. (■) 1148 kHz, 445.5 Da; (●) 844.5 kHz, 445.5 Da; (▲) 844.5 kHz, 134.2 Da.

is presumably because the ion velocity is at a maximum through the center of the trap and so the ion spends less time in the center than at the "turn-around" point of the ion's trajectory, where its velocity decreases to zero and then reverses direction.

Effect of Drive Frequency on Ion Cloud Size. IRMPD was performed on the *n*-butylbenzene ion generated by EI. Again, the q_z value was varied and the fragmentation efficiency was recorded. This was done at two different drive frequencies: 844.5 and 1148 kHz. The results are shown in Figure 6a, where the squares represent data points taken at 1148 kHz, and the triangles represent data points taken at 844.5 kHz. Curves of the same type/color represent equal laser powers. Comparing the results from using different frequency at the same laser power, the

fragmentation efficiency at the higher drive frequency is significantly greater than at the lower frequency. This result makes sense because well depth varies as the square of trapping frequency (eq 6), so at higher frequencies, ions are in a smaller ion cloud. A true comparison of the effect of two different frequencies on ion cloud size can be made, because all other experimental parameters are the same. That is, at both frequencies the ion requires the same number of photons to dissociate, because the trap pressure and the calculated collision frequency were equal at both frequencies. The only difference, therefore, is the ion cloud size, which is affecting laser overlap and the photon absorption rate. Trajectory modeling (Figure 6b) shows that the most probable ion position at a q_z of 0.30 is at a radius of 0.35 mm at 844.5 kHz, while this position is 0.26 mm at 1148 kHz.

Effect of Mass on Ion Cloud Size. Unfortunately an experiment to probe the ion cloud size for ions of different masses is difficult to design. Observing the IRMPD fragmentation efficiency at different q_z values for different size ions does not allow conclusions about relative ion cloud size to be drawn, because larger ions will require more photons to be absorbed for dissociation. Thus, the positional dependence of fragmentation efficiency is convoluted with different energetic requirements for dissociation. One can hypothesize that since mass is in the numerator in eq 6 that larger ions will be at smaller radii than less massive ions when compared at the same q_z value. Naturally, however, when different size ions are stored in the QITMS at the same time, they have different q_z values. In this second case, one expects the smaller ions at higher q_z to be closer to the center of the trap. Fragmentation efficiency vs q_z curves for the peptides GHK and FLLVPLG were qualitatively similar to those obtained for tetracycline. An attempt was made to normalize the different energetic requirements of different size ions to a collision-induced dissociation breakdown curve experiment and/or to the number of degrees of freedom of each ion, without success as of yet. Trajectory calculations, however, can illuminate the situation, as is shown in Figure 6b. The 134.2 Da *n*-butylbenzene ion, plotted as triangle data points, is most likely found at a radius of 0.45 mm, as opposed to the 445.5 Da tetracycline ion, shown in circles, which has a highest probability at 0.35 mm.

Conclusions

The size of the ion cloud in a QITMS has a noticeable effect on IRMPD dissociation efficiency. Maximal overlap of the ion cloud with the highest flux volume of the laser beam can be obtained by optimizing several parameters that determine the magnitude of the restoring force pushing the ion toward the center of the trap. From the equation for the depth of the pseudopotential well (eq 6), the most important factors are trapping voltage, trapping frequency, and ion mass. Ion mass obviously is not a parameter that can be optimized, although it is interesting that a higher mass-to-charge ion (e.g., a protein) should actually experience better laser overlap then a smaller peptide, if both ions were irradiated while at the same q_z value. Trapping frequency is generally not a parameter that may be adjusted easily; however, this study suggests that when one is designing an instrument for IRMPD, a higher frequency drive voltage can be advantageous, especially when laser power is seen to be a limiting factor in the experiment. Finally, the amplitude of the trapping voltage applied during IRMPD, or the q_z value, plays an important role. Because rf trapping instruments are commonly operated at high bath gas pressures, the rate of collisional cooling competes with the rate of energy deposition through photon absorption. Therefore the q_z value may be adjusted to higher values to allow maximum activation of the ion. However, a high q_z value increases the low mass cutoff and lower mass product ions may not be trapped. Loss of low *m*/*z* product ions may be undesirable, and so as in most experiments, a compromise must be reached between the quality of the data output and the experimental time and expense. Experimental time refers to parameters such as laser excitation time and ion gating time, which depends on trapping efficiency and thus bath gas pressure. Expense refers to cost and thus power of the laser. A possible operating procedure to address this q_z issue would be to start IRMPD at a high q_z value and decrease the rf voltage over the course of laser irradiation, so that successive generations of product ions could be formed and continue to be trapped in the instrument.

Acknowledgment. This work was supported by National Science Foundation Grant No. CHE-0431825.

References and Notes

(1) Dunbar, R. C. *J. Am. Chem. Soc.* **1971**, *93*, 4354.
(2) Uechi, G. T.; Dunbar, R. C. *J. Chem. Phys.* **1990**, *93*, 1626.
(3) Dunbar, R. C. *J. Chem. Phys.* **1989**, *90*, 7369.
(4) Black, D. M.; Payne, A. H.; Glish, G. L. *J. Am. Soc. Mass Spectrom.* **2006**, *17*, 932.
(5) Stephenson, J. L.; Booth, M. M.; Shalosky, J. A.; Eyler, J. R.; Yost, R. A. *J. Am. Soc. Mass Spectrom.* **1994**, *5*, 886.
(6) Vining, B. A.; Li, G.-Z.; Marshall, A. G. *J. Am. Soc. Mass Spectrom.* **1998**, *9*, 925.
(7) Cleven, C. D.; Cooks, R. G.; Garrett, A. W.; Nogar, N. S.; Hemberger, P. H. *J. Phys. Chem.* **1996**, *100*, 40.
(8) Boué, S. M.; Stephenson, J. L.; Yost, R. A. *Rapid Commun. Mass Spectrom.* **2000**, *14*, 1391.
(9) Gabryelski, W.; Li, L. *Rev. Sci. Instrum.* **1999**, *70*, 4192.
(10) Little, D. P.; Speir, J. P.; Senko, M. W.; O'Connor, P. B.; McLafferty, F. W. *Anal. Chem.* **1994**, *66*, 2809.
(11) Thompson, M. S.; Cui, W.; Reilly, J. P. *Angew. Chem., Int. Ed.* **2004**, *43*, 4791.
(12) Cui, W.; Thompson, M. S.; Reilly, J. P. *J. Am. Soc. Mass Spectrom.* **2005**, *16*, 1384.
(13) Colorado, A.; Shen, J. X.; Vartanian, V. H.; Brodbelt, J. *Anal. Chem.* **1996**, *68*, 4033.
(14) Tsybin, Y. O.; Witt, M.; Baykut, G.; Kjeldsen, F.; Hakansson, P. *Rapid Commun. Mass Spectrom.* **2003**, *17*, 1759.
(15) Pivonka, N. L.; Kaposta, C.; Bruemmer, M.; von Helden, G.; Meijer, G.; Woste, L.; Neumark, D. M.; Asmis, K. R. *J. Chem. Phys.* **2003**, *118*, 5275.
(16) Oomens, J.; Meijer, G.; Helden, G. v. *J. Phys. Chem. A* **2001**, *105*, 8302.
(17) Oomens, J.; Moore, D. T.; Helden, G. v.; Meijer, G.; Dunbar, R. C. *J. Am. Chem. Soc.* **2004**, *126*, 724.
(18) Putter, M.; von Helden, G.; Meijer, G. *Chem. Phys. Lett.* **1996**, *258*, 118.
(19) von Helden, G.; Holleman, I.; Putter, M.; Meijer, G. *Nucl. Instrum. Methods Phys. Res. B* **1998**, *144*, 211.
(20) Payne, A. H.; Glish, G. L. *Anal. Chem.* **2001**, *73*, 3542.
(21) Crowe, M. C.; Brodbelt, J. *J. Am. Soc. Mass Spectrom.* **2004**, *15*, 1581.
(22) Gardner, M. W.; Vasicek, L. A.; Shabbir, S.; Anslyn, E. V.; Brodbelt, J. S. *Anal. Chem.* **2008**, *80*, 4807.
(23) *Quadrupole Ion Trap Mass Spectrometry*, 2nd ed.; March, R. E., Todd, J. F. J., Eds.; John Wiley & Sons, Inc.: Hoboken, NJ, 2005; Vol. 165, p 346.
(24) March, R. E. Quadrupole Ion Trap Mass Spectrometry. In *Encyclopedia of Analytical Chemistry*; Meyers, R. A., Ed.; John Wiley & Sons Ltd.: Chichester, 2000; Vol. 13, p 11848.
(25) March, R. E. *J. Mass Spectrom.* **1997**, *32*, 351.
(26) Stafford, G. C. J.; Kelley, P. E.; Syka, J. E. P.; Reynolds, W. E.; Todd, J. F. J. *Int. J. Mass Spectrom. Ion Process.* **1984**, *60*, 85.
(27) Louris, J. N.; Cooks, R. G.; Syka, J. E. P.; Kelley, P. E.; Stafford, G. C.; Todd, J. F. J. *Anal. Chem.* **1987**, *59*, 1677.
(28) March, R. E.; Todd, J. F. J. *Practical Aspects of Ion Trap Mass Spectrometry*; CRC Press: New York, 1997; Vol. 1−3.
(29) Major, F. G.; Dehmelt, H. G. *Phys. Rev.* **1968**, *170*, 91.
(30) Dehmelt, H. G. Radiofrequency Spectroscopy of Stored Ions. I. Storage. In *Advances in Atomic and Molecular Physics*; Bates, D. R., Estermann, I., Eds.; Academic Press: New York, 1967; Vol. 3, p 53.

(31) Williams, J. D.; Cooks, R. G.; Syka, J. E. P.; Hemberger, P. H.; Nogar, N. S. *J. Am. Soc. Mass Spectrom.* **1993**, *4*, 792.
(32) Goeringer, D. E.; McLuckey, S. A. *Int. J. Mass Spectrom.* **1998**, *177*, 163.
(33) Payne, A. H.; Glish, G. L. "Thermally-Assisted Infrared Multiphoton Photodissociation in a Quadrupole Ion Trap"; The 49th ASMS Conference on Mass Spectrometry and Allied Topics: Chicago, IL, 2001.
(34) Remes, P. M.; Glish, G. L. *Int. J. Mass. Spectrom* **2007**, *265*, 176.
(35) O'Conner, P. B. C.; Catherine, E.; Earle, William, E. *J. Am. Soc. Mass Spectrom.* **2002**, .
(36) Schwartz, J.; Zhou, X.; Bier, M. E. Method of increasing the dynamic range and sensitivity of a mass spectrometer. In *USPO*; Finnigan Corporation: US, 1996.
(37) Dahl, D. A. SIMION 3D, 7th ed.; Idaho National Engineering Laboratory: Idaho Falls, 1999.
(38) Manura, D. Collision Model HS1 http://www.simion.com/info/Collision_Model_HS1, 2007.
(39) Quarmby, S. T.; Yost, R. A. *Int. J. Mass Spectrom.* **1999**, *190/191*, 81.
(40) Asano, K. G.; Goeringer, D. E.; McLuckey, S. A. *Int. J. Mass Spectrom.* **1999**, *185/186/187*, 207.
(41) Plass, W. R.; Cooks, R. G. *J. Am. Soc. Mass Spectrom.* **2003**, *14*, 1348–1359.

JP808955W